

Dwarf planet Ceres: Ellipsoid dimensions and rotational pole from Keck and VLT adaptive optics images [☆]



J.D. Drummond ^{a,*}, B. Carry ^b, W.J. Merline ^c, C. Dumas ^d, H. Hammel ^e, S. Erard ^f, A. Conrad ^g, P. Tamblyn ^c, C.R. Chapman ^c

^aStarfire Optical Range, Directed Energy Directorate, Air Force Research Laboratory, Kirtland AFB, NM 87117-577, USA

^bIMCCE, Observatoire de Paris, CNRS, 77 av. Denfert Rochereau, 75014 Paris, France

^cSouthwest Research Institute, 1050 Walnut St. # 300, Boulder, CO 80302, USA

^dESO, Alonso de Córdova 3107, Vitacura, Casilla 19001, Santiago de Chile, Chile

^eAURA, 1200 New York Ave. NW, Suite 350, Washington, DC 20005, USA

^fLESIA, Observatoire de Paris, CNRS, UPMC, Université Paris-Diderot, 5 place Jules Janssen, 92195 Meudon, France

^gMax-Planck-Institut fuer Astronomie, Koenigstuhl 17, D-69117 Heidelberg, Germany

ARTICLE INFO

Article history:

Received 7 December 2013

Revised 13 March 2014

Accepted 14 March 2014

Available online 5 April 2014

Keywords:

Adaptive optics

Asteroid Ceres

Asteroids

ABSTRACT

The dwarf planet (1) Ceres, the largest object between Mars and Jupiter, is the target of the NASA Dawn mission, and we seek a comprehensive description of the spin-axis orientation and dimensions of Ceres in order to support the early science operations at the rendezvous in 2015. We have obtained high-angular resolution images using adaptive optics cameras at the W.M. Keck Observatory and the ESO VLT over ten dates between 2001 and 2010, confirming that the shape of Ceres is well described by an oblate spheroid. We derive equatorial and polar diameters of 967 ± 10 km and 892 ± 10 km, respectively, for a model that includes fading of brightness towards the terminator, presumably linked to limb darkening. These dimensions lie between values derived from a previous analysis of a subset of these images obtained at Keck by Carry et al. (Carry et al. [2008]. *Astron. Astrophys.* 478 (4), 235–244) and a study of Hubble Space Telescope observations (Thomas et al. [2005]. *Nature* 437, 224–226). Although the dimensions are 1–2% smaller than those found from the HST, the oblateness is similar.

We find the spin-vector coordinates of Ceres to lie at $(287^\circ, +64^\circ)$ in equatorial EQJ2000 reference frame ($346^\circ, +82^\circ$ in ecliptic ECJ2000 coordinates), yielding a small obliquity of 3° . While this is in agreement with the aforementioned studies, we have improved the accuracy of the pole determination, which we set at a 3° radius.

Published by Elsevier Inc.

1. Introduction

The largest asteroid, the dwarf-planet (1) Ceres, remains an enigma more than two centuries after its discovery in 1801 (see the review by Rivkin et al., 2011). Its diameter of ≈ 1000 km is twice that of any other asteroid, and concentrates over a fifth of all the matter between Mars and Jupiter (Kuchynka and Folkner, 2013). After half a century of photometric and spectroscopic

studies, critical questions remain about Ceres' surface and interior composition with respect to differentiation, bulk composition, and state of hydration. The NASA Discovery mission Dawn (Russell et al., 2007), on its way to Ceres after its encounter with Asteroid (4) Vesta in 2011 (Russell et al., 2012), has been designed to answer these questions.

Earth-based observations over decades have indeed left us with a puzzling picture. Owing to its albedo and visible and near-infrared spectrum, Ceres was initially linked with dark carbonaceous chondrite meteorites (see Chapman et al., 1973, for instance). In the late 1970s, the detection of a spectral absorption around $3 \mu\text{m}$ in its reflectance spectrum was interpreted as a signature of water ice (see Lebofsky, 1978; Feierberg et al., 1980, among others), although this was not a consensus interpretation; different assemblages of hydrated minerals have also been proposed (e.g., King et al., 1992; Milliken and Rivkin, 2009). Water ice received

[☆] Based on observations collected at the European Southern Observatory, Paranal, Chile – 072.C-0092, 075.C-0329 & 080.C-0881 – and at the W.M. Keck Observatory, which is operated as a scientific partnership among the California Institute of Technology, the University of California and the National Aeronautics and Space Administration. The Observatory was made possible by the generous financial support of the W.M. Keck Foundation.

* Corresponding author.

E-mail address: jack.drummond@kirtland.af.mil (J.D. Drummond).

strong support when A'Hearn and Feldman (1992) reported the detection of OH escaping from Ceres. Even though this detection was marginal and could not be confirmed until very recently (Rousselot et al., 2011; Küppers et al., 2014) it motivated thorough modeling studies of the internal structure of Ceres and of its possible water regime (Fanale and Salvail, 1989; McCord and Sotin, 2005). Even the determination of the mass and volume, and hence density, of Ceres have been subject to discrepant estimates (see the review by Carry, 2012). Based on these (sometimes controversial) observational lines of evidence, several internal structure models are allowed, ranging from a homogeneous body to a fully differentiated proto-planet with a sub-surface shell of water ice (Zolotov, 2009; Castillo-Rogez and McCord, 2010). Because different internal structures would yield different polar-to-equator oblateness values, much effort has been made to determine the dimensions of Ceres (Thomas et al., 2005; Carry et al., 2008; Drummond and Christou, 2008). Thus the size and shape (oblateness), as determined from direct observations, impact estimates of density and internal structure, and are even relevant to any possible presence of water. For example, Thomas et al. (2005) inferred differentiation and the presence of water ice from the shape alone.

With the imminent arrival of the NASA Dawn mission to Ceres in 2015, many of these questions are expected to be answered. However, the scientific operations in the early stages of the encounter require an a priori knowledge of the spin axis and, to a lesser extent, of the dimensions of Ceres. Ceres' spin axis has been difficult to determine from any photometric technique because its lightcurve amplitude has always been small, regardless of observing geometry. This could be the result of a spherical object, where any amplitude might be the result of albedo variations (Li et al., 2006) rather than a difference in equatorial dimensions, or to a small obliquity (the angle between the rotational and orbital poles). All lightcurve inversion techniques, for spin and/or shape determination, assume that lightcurve variations are linked with the apparent change of shape on the plane of the sky, that is, they assume a homogeneous albedo. However, the optical lightcurves of Ceres have been shown to be directly related to the albedo markings on its surface (Li et al., 2006), like Vesta, and unlike the vast majority of asteroids, and this is why neither the spin axis nor the 3-D shape of Ceres has been derived from lightcurves, although tens of epochs have been acquired over decades.

Carry et al. (2008) used KOALA (Kaasalainen et al., 2011; Carry et al., 2010b, 2012) to derive the shape and spin pole for Ceres, but, as discussed above, a problem with KOALA is that the low amplitude lightcurves produced by a near-oblate object always observed near its equatorial plane provide little constraint. Moreover, since the limb profiles of Ceres show an ellipsoid curve, with no noticeable deviations from an ellipse (Carry et al., 2008), we examine all of our resolved images with the simplest assumption – that Ceres is a triaxial ellipsoid. We compare our results for Ceres' pole and dimensions to four previous studies, a stellar occultation in 1984 (Millis et al., 1987), a summary of previous AO observations (Drummond and Christou, 2008), and in particular to Hubble Space Telescope (HST) observations (Thomas et al., 2005) and to AO images from the W.M. Keck Observatory (Carry et al., 2008).

Most of our observations use arguably the best instrument on Earth or in space to make the highest resolution images possible. The 10 m diameter mirror of Keck gives the largest aperture currently available for imaging and, when combined with its extraordinary oversampling at 0.01"/pixel (two times oversampled), it allows us to acquire unprecedented imaging of large main-belt asteroids. In the best circumstances reported in this paper, our images have 18 resolution elements across Ceres (265 resolution elements on the disk) and are 80 pixels across, covering the face of Ceres with more than 5000 pixels. Our techniques were

demonstrated on (21) Lutetia (Drummond et al., 2010; Carry et al., 2010) prior to the flyby of the Rosetta spacecraft. At the time, Lutetia was near the lower limit in angular size for our technique ($\sim 0.10''$), while Ceres is nearly eight times larger in size. Our results on Lutetia were validated during the Rosetta flyby (Carry et al., 2012) and showed that our triaxial dimensions were good to 2%, with RMS deviation in actual surface topography of only 2 km on this 100 km body. The 10 year span over which we report data allows the opportunity to sample the asteroid over a range of sub-Earth latitudes and longitudes on Ceres and represents the most comprehensive imaging data set ever acquired. Our intent is to solidify the measured size, shape, and pole of Ceres as the Dawn spacecraft approaches the dwarf planet.

2. Additional observations

At an apparent size of about 0.8" at opposition, Ceres can be angularly resolved only by the HST from space or large ground-based telescopes equipped with adaptive-optics (AO) such as the Lick 3 m Shane telescope, the Keck II telescope, the Gemini twin telescopes, or the European Southern Observatory (ESO) Very Large Telescope. For this study we assemble images we acquired at the Keck and VLT from 2001 to 2010 on 10 nights at 32 different epochs, spanning a variety of Sun–Ceres–Earth geometries (Table 1).

Images at the Keck telescope were obtained with the NIRC2 infrared camera (van Dam et al., 2004) at a pixel resolution of 9.942 mas/pixel through a Kp-filter (with one exception, a J filter in 2002). We prefer these images to those taken at shorter wavelength (e.g., J- or H-band) because of the higher quality of AO correction with increasing wavelength. Images from the VLT were taken with the NACO camera (Lenzen et al., 2003; Roussel et al., 2003), with the Ks-filter and the S13 pixel scale of 13.27 mas/pixel.

All the 295 raw images were reduced in the usual manner with bad-pixel removal, sky background subtraction, flat-fielding, etc. We present examples of these images in Fig. 1.

3. Modeling the shape of Ceres

We use the Parametric Blind Deconvolution (PBD) method (e.g., Drummond et al., 1998, 2009a) to measure the apparent size and orientation of Ceres. The details of our technique have been extensively described in our studies of previous asteroids (see Drummond, 2000; Conrad et al., 2007; Drummond and Christou, 2008; Drummond et al., 2009a, 2010; Merline et al., 2013), but briefly, for each image, in the Fourier plane, we measure the dimensions of the major (α) and minor (β) axes and the orientation (position angle of long axis: PA) of the projected ellipse of Ceres on the plane of the sky, assuming that it is smooth and flatly illuminated from limb to terminator. These three parameters comprise the observables used in a non-linear least squares fit for six unknowns, the three ellipsoid dimensions and the three Euler angles (rotational phase, latitude of the sub-Earth point (SEP), and position angle of the line of nodes – the intersection of the equatorial plane and the plane of the sky) which describe the orientation of each ellipse. Minimizing the differences between the measured and predicted apparent sizes and orientations as a function of rotational phase yield the full ellipsoid dimensions and the location of the spin axis. We use the sidereal period from Chamberlain et al. (2007) of 9.074 170 h (with an uncertainty of 1 in the last digit) to tie all of the observations together. We consider two possible shapes for Ceres, a triaxial ellipsoid defined by three diameters ($a > b > c$) and a biaxial ellipsoid, specifically an oblate spheroid, where $a = b$.

Fig. 2 shows the fit for the night with the most data. The data at other times are much more sparse, but we plot in Fig. 3 the

Table 1
Observing Log. For each date of observation we list the observing site, the camera and the filter (including the central wavelength λ_0), the exposure time, the number of epochs (n), where each epoch is the average of several measurements (i.e., images), the equatorial coordinates of Ceres (RA, December), the solar phase angle (ω), the position angle of the Sun at the asteroid (NTS, used for orientation), and the distance from the Earth to Ceres (Δ).

Date	Site	Camera	Filter	λ_0 (μm)	exp (s)	n	RA ($^\circ$)	December ($^\circ$)	ω ($^\circ$)	NTS ($^\circ$)	Δ (AU)
2001 August 5	Keck	NIRC2	Kp	2.124	0.05	1	281.9	-30.9	11.1	253.2	2.019
2002 August 4	Keck	NIRC2	J	1.248	0.5	1	21.4	-4.9	18.3	73.4	2.407
2002 September 22	Keck	NIRC2	Kp	2.124	1.0	14	18.3	-8.5	6.9	112.5	1.982
2002 September 28	Keck	NIRC2	Kp	2.124	1.0	2	17.1	-9.0	6.0	131.1	1.966
2004 January 14	VLT	NACO	Ks	2.15	0.5	4	110.3	+30.5	3.8	333.3	1.627
2005 May 9	VLT	NACO	Ks	2.15	2.0	3	228.0	-8.5	3.4	12.8	1.687
2007 November 11	VLT	NACO	Ks	2.15	2.0	4	46.5	+8.1	3.2	175.5	1.832
2009 June 7	Keck	NIRC2	Kp	2.124	0.6	1	165.1	+17.9	23.1	291.8	2.478
2010 March 30	Keck	NIRC2	Kp	2.124	0.18	1	272.1	-21.5	20.9	88.8	2.463
2010 May 27	Keck	NIRC2	Kp	2.124	0.18	1	272.2	-24.1	9.1	90.6	1.879

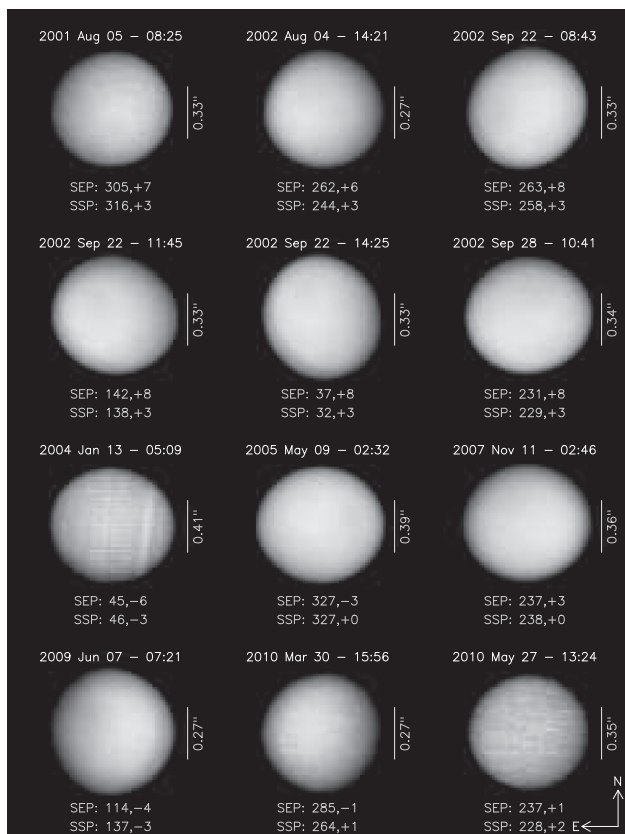


Fig. 1. Examples of images of Ceres used in the analysis. For each image, the date and mid-exposure time (in UT) is reported, together with the planetocentric coordinates of the sub-Earth and sub-solar points (SEP and SSP, respectively). All images are scaled to the same true size, with an apparent size scale bar drawn next to each, and all are oriented with celestial north up and east to the left. Apparent variegations on the disk, particularly for 2004 January 13, are not real, but are artifacts of the deconvolution.

residuals between our model and all observations, as well as including the average ellipse parameters (kindly provided by P. Thomas) measured from 207 HST images obtained at 0.220–0.555 μm over four intervals between 2003 December 28 and 2004 January 24 (Thomas et al., 2005), and from a stellar occultation in 1984 (Millis et al., 1987). The diameters for both the triaxial ellipsoid and oblate spheroid assumptions are listed in Table 2, where the uncertainties are fitting errors only.

3.1. Limb darkening and terminator fade

From previous analyses of our technique for size measurement on asteroids, Saturn's satellites, and simulations (Drummond et al.,

2009b; Carry, 2009; Carry et al., 2010; Merline et al., 2013) we have found that our systematic uncertainty with 8–10 m telescopes ranges from 3% to 4% at the small end of the range of angular sizes that we can measure (0.08–0.09 $''$) to 1% at Ceres' size. One possible source for this systematic uncertainty is the violation of one of our assumptions, that the object is evenly illuminated to its edge and to the terminator. While heretofore we have explicitly included the geometry of the terminator in our analysis, we have not addressed the possibility that limb-darkening may affect our measurements of the true size, especially at higher solar phase angles. The clear trend of the residuals in our fits with solar phase angles (Fig. 3) suggests a limb-darkening-like phenomenon on Ceres that would lead to underestimating its size at higher solar phase angles, particularly its apparent major axis.

The non-uniform appearance of Ceres can be seen in Fig. 1, and a strong photometric gradient across the face of Ceres for the images obtained on 2002 September 22, reported and shown by Carry et al. (2008), supports the notion of uneven illumination even at a solar phase angle of only 7 $^\circ$. Others have evaluated the apparent level of limb-darkening on Ceres and also found it to be significant (Parker et al., 2002; Li et al., 2006).

Because Ceres has a small obliquity the subsolar point varies far more from the sub-Earth point in longitude than in latitude, with excursions in longitude of up to $\pm 25^\circ$ compared to no more than 6 $^\circ$ in latitude. Thus, at large solar phase angles, the difference between the subsolar and sub-Earth points is mostly in Ceres planetocentric longitude. This, together with the oblate spheroid shape of Ceres, means that the terminator truncates the apparent long axis more than the short axis at higher solar phase angles. Since the impact of the limb-darkening-like phenomenon is greatest in the direction of the terminator, we call this a 'terminator fade'.

We seek here not to solve for the resolved-disk limb-darkening parameters, but instead use a simple model to estimate the effect of this terminator fade on the apparent size of the disk itself, at various phase angles. Such refinement has not been required for the other asteroids we have studied to date (e.g., Drummond et al., 2009a, Drummond et al., 2010; Merline et al., 2013), most likely because of their much smaller apparent diameter and the low phase angles at which they are usually observed. The apparent diameter of Ceres of 0.6 $''$ to 0.8 $''$, however, spreads over many pixels in the images, allowing this terminator fade to be detected.

Although both Lommel-Seeliger and Lambertian phase functions lead to a soft terminator, the latter shows strong limb darkening even at a solar phase angle of zero, which violates our assumptions. Our PBD model assumes no limb darkening and is closer to following a Lommel-Seeliger phase function. Fitting airless bodies for size in the Fourier plane (PBD) is much more sensitive to edges than photometric variation across the visible disk, and we simply increase the apparent size as measured in the Fourier

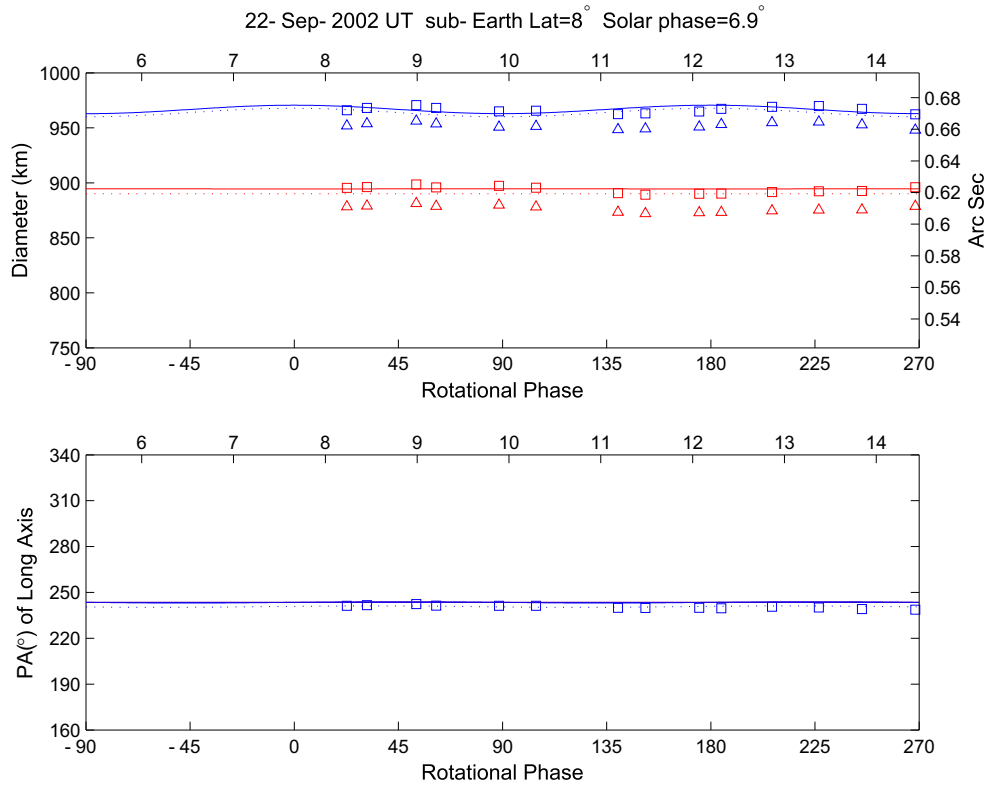


Fig. 2. Triaxial ellipsoid fit to measured ellipse parameters for Ceres on 2002 September 22 from Keck. Plots for an oblate spheroid would be very similar, the only difference being that the upper line in each plot would be straight and not sinusoidal. Squares are measured axes diameters, corrected with Eq. (1) from the actually observed parameters displayed as triangles, blue for the long axes and red for the short. The solid lines are the predictions for the projected ellipses from the triaxial ellipsoid parameters in Table 2 and the dashed lines are for the ellipse parameters for the terminator ellipse (Drummond et al., 1985; Drummond, 2000). The data should lie approximately midway between the dashed and solid lines. The lower subplot shows the same information in the same way for the position angle of the long axis. The solid line across the lower subplot is the line of nodes where the asteroid’s equator intersects the plane of the sky. This figure is corrected for light time travel, i.e., the plot is in the body-centered time frame. (For interpretation of the references to colour in this figure legend, the reader is referred to the web version of this article.)

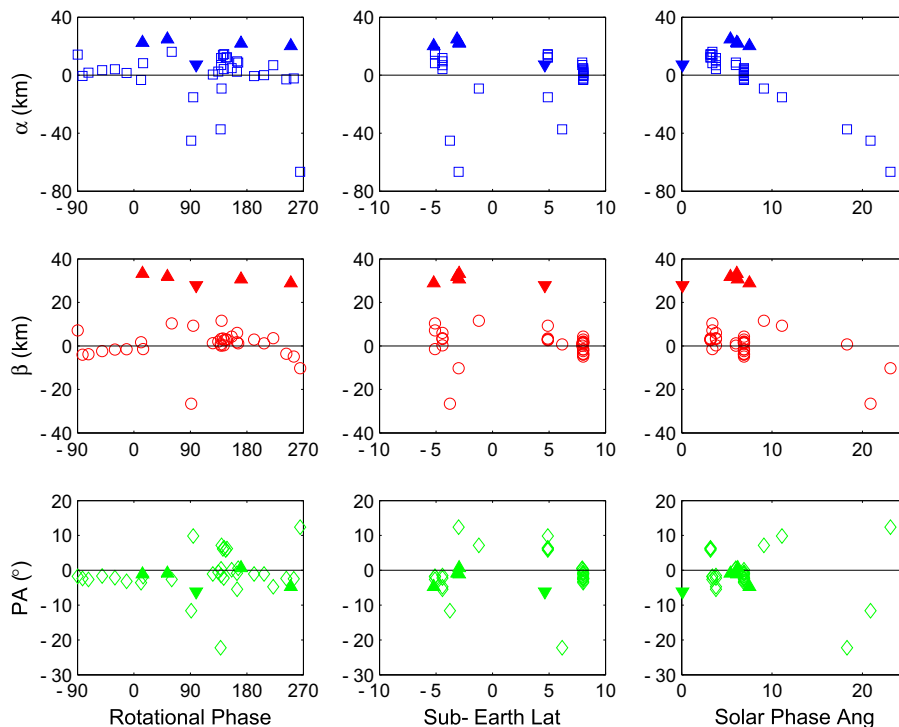


Fig. 3. Residuals for the oblate spheroid model, without terminator fade corrections, for all AO observations. AO measurements are open symbols, HST measurements Thomas et al., 2005) are solid upward point triangles, and the occultation (Millis et al., 1987) ellipse is the downward pointing triangle at zero solar phase angle.

Table 2
Solutions for Ceres' dimensions (see text).

a (km)	b (km)	c (km)	k	
<i>Without terminator fade</i>				
954 ± 5	951 ± 6	877 ± 3	–	Tri ell
953 ± 3	953 ± 3	878 ± 3	–	Obl sph
<i>With terminator fade</i>				
971 ± 6	963 ± 6	893 ± 4	0.19 ± 0.03	Tri ell
967 ± 4	967 ± 4	892 ± 4	0.18 ± 0.03	Obl sph

plane, to account for terminator fading, to arrive at a true illuminated area.

To attempt to correct for this effect, from geometric considerations, we introduce a simple function that relates the actual size of the illuminated disk to the apparent one, based on our AO observations. We relate the observed ellipses (O indices) to the true illuminated ellipsoid (M indices) dimensions with

$$\begin{aligned} \alpha_O &= \alpha_M - kr \sin \omega \cos \delta \\ \beta_O &= \beta_M - kr \sin \omega \sin \delta, \end{aligned} \quad (1)$$

where k is a constant (larger for stronger terminator fading), r is the length of the radius vector to the sub-Sun point, $r \sin \omega$ is the distance from the center to the sub-Sun point in the plane of the sky, and δ is the angle between the Sun and the asteroid's computed illuminated major axis. See Appendix A. Although not to the extreme as depicted in A, using Eq. (1) to correct observed or measured ellipses to true illuminated ellipses, and fitting Ceres observations for k and the ellipse parameters simultaneously, accounts for the discrepancy in projected dimensions at large solar phase angles ($\omega > 12^\circ$), as can be seen by comparing Fig. 3 for no correction to Fig. 4.

We list in Table 2 the diameters for a triaxial ellipsoid and an oblate spheroid, with and without terminator fade, and the RMS residuals for the oblate spheroid model are given in Table 3. In Table 4 we give the mean difference between our projected ellipse

Table 3
RMS residuals of the projected axes (α and β) and orientation (PA) without and with terminator fade for oblate spheroid.

	Without	With
α (km)	17.6	3.4
β (km)	6.6	7.2
PA ($^\circ$)	6.2	6.2

Table 4
Average difference between AO (oblate spheroid) projected ellipses (α , β and PA) and HST and occultation ellipses, without and with terminator fade.

	AO-HST		AO-Occ	
	Without	With	Without	With
α (km)	22	8	7	–7
β (km)	31	17	28	14
PA ($^\circ$)	–2	–1	–6	–6

parameters for the oblate spheroid case and the apparent ellipses measured by HST, and as determined for the stellar occultation, where it can be seen that including terminator fading improves the agreement for both axes, especially the long one.

The degree of terminator fade we find on Ceres ($k = 0.19 \pm 0.03$) is larger than on another recently studied asteroid, (52) Europa (Merline et al., 2013), for which we find $k = 0.12 \pm 0.08$. The much higher uncertainty in the determination of terminator fade for Europa with our method (as indicated by the 67% uncertainty of k , compared to 17% for Ceres) is the result of two factors, the small solar phase angles (and small range) of the two sets of observations (5.5° and 13.3°), and the smaller angular size of the disk in the AO images for Europa. Thus, terminator fade is easier to discern and measure on the much larger Ceres. Because k cannot be determined reliably from our Europa data, and because our Europa observations are within a phase regime where use of k in the model is less important in size determination, our published

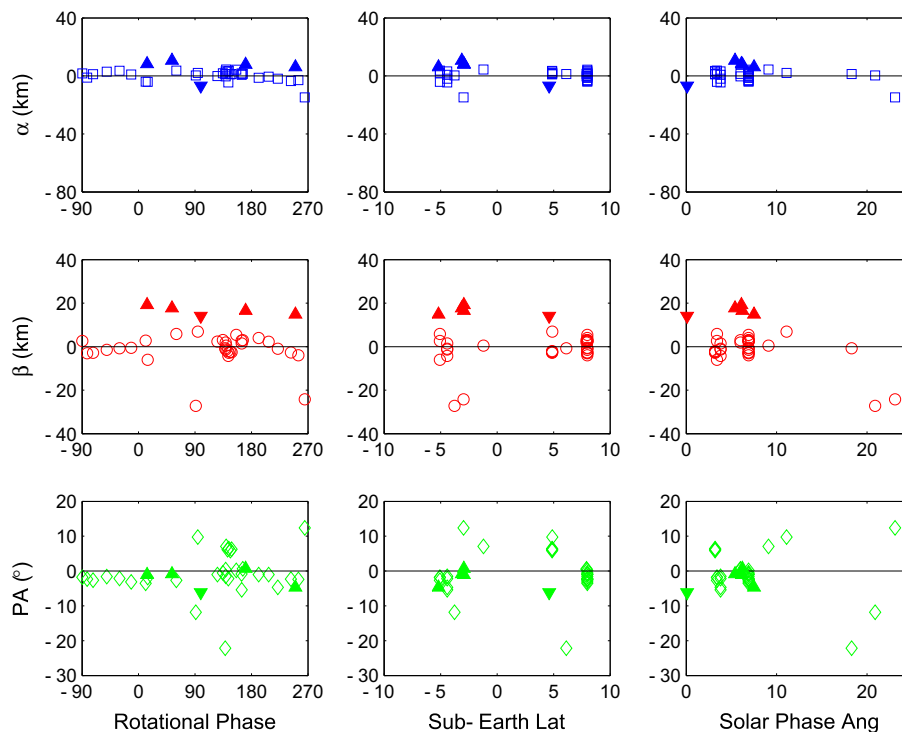


Fig. 4. Same as Fig. 3, but for the oblate spheroid model with terminator fade corrections using Eq. (1).

analysis does not include terminator fade for Europa. We cannot say whether terminator fading is any different on Europa than on Ceres, but our work demonstrates that including limb darkening in the analysis is more important for studies of well-resolved objects like Ceres than for less well-resolved objects such as our observations of Europa.

3.2. The dimensions of Ceres

Because there is no statistically significant difference between the a and b diameters in a triaxial fit, we adopt the oblate spheroid solution. Although we note and correct for terminator fading, we may continue to have other systematics effects as well (such as pixel size on the plane of the sky or incomplete sub-sampling on the pixel grid). As we have done in previous papers, therefore, we determine our final uncertainties by quadratically adding our current estimated systematic uncertainties of 1% of the diameters and our formal model fitting errors to arrive at our final estimates for sizes and uncertainties of $a = b = 967 \pm 10$ and $c = 892 \pm 10$ km.

We compare this adopted solution with other determinations from the stellar occultation (Millis et al., 1987), from HST (Thomas et al., 2005), and from Keck (Carry et al., 2008; Drummond and Christou, 2008) imaging in Table 5. Accounting for terminator fading increases our dimensions of Ceres by 14 km compared to no limb darkening, and makes the c diameter closest to, but now larger than, Carry et al. (2008), who did not include limb-darkening in their analysis. If they had, the dimensions they derived would have been even closer to the other values in Table 5. (Thomas et al., 2005) did not include limb darkening in their analysis since the solar phase angle was so small (6°), making the terminator indistinguishable from the edge. The occultation and HST c dimensions are similar, around 15 km larger than our adopted value with limb darkening.

Our equatorial diameter, with terminator fading, is 7–8 km larger than the occultation and Carry et al. (2008) dimensions, but 8 km smaller than the HST dimension in Table 5. Since some of our measurements were close in time to the HST observations in early 2004, the difference in dimensions between the HST measurements and our results must be due to the apparent dimensions of Ceres as measured, and not to geometry. In the end, we find, particularly in the polar diameter, that Ceres is smaller than suggested by HST measurements. Although the oblateness (a/c) found here of 1.08 ± 0.02 is at the high end of the range from the studies in Table 5, considering that all of the oblateness errors calculated from Table 5 overlap, there is overall agreement in oblateness with a value of 1.07 calculated from the mean.

4. Rotational pole

The coordinates of the rotation pole for both models listed in Table 2 are the same, and are given in Table 6 as our adopted rotational pole for Ceres. In addition, as a check, we apply two methods of intersecting great circles to derive Ceres' pole since these

Table 5
Summary of Ceres' dimensions.

$a = b$ (km)	c (km)	D (km)	Ref.
967 ± 10	892 ± 10	941 ± 6	1
960 ± 5	906 ± 9	942 ± 4	2
974.6 ± 3.6	909.4 ± 3.2	952 ± 2	3
973 ± 7	908 ± 8	951 ± 4	4
959.4 ± 4.6	888.8 ± 4.2	935 ± 3	5

References. 1: Present study. 2: Millis et al., 1987. 3: Thomas et al., 2005. 4: Drummond and Christou, 2008. 5: Carry et al., 2008.

Table 6

Coordinates of Ceres' spin vector from different methods: ellipsoid/spheroid modeling, great circles (GC) a and b , and control point (CP).

EQJ2000		ECJ2000		σ	Method	Refs.
(RA)	(December)	(λ)	(β)			
287°	$+64^\circ$	346°	$+82^\circ$	3°	Ellipsoid	1
288°	$+60^\circ$	329°	$+80^\circ$	12°	GC _a	1
288°	$+58^\circ$	323°	$+78^\circ$	6°	GC _b	1
291°	$+59^\circ$	332°	$+78^\circ$	5°	CP	2
293°	$+63^\circ$	351°	$+80^\circ$	4°	GC _a	3
288°	$+66^\circ$	4°	$+83^\circ$	5°	CP	4

References. 1: Present study. 2: Thomas et al. (2005). 3: Drummond and Christou (2008). 4: Carry et al. (2008).

methods are independent of the dimensions and rotation of the body and therefore provide an independent determination. Drummond and Christou (2008) found the rotational pole as the average of the intersections of the great circles from the position of the asteroid each night in the direction of the minor axes (hereafter method a). The number of intersections to average is $N = n! / 2(n-2)!$, where n is the number of positions.

The second method (b) follows Li et al. (2011), who pointed out that of the two angles required for the location of the pole, the position angle of the line of nodes and the sub-Earth point latitude, the latter is by far the least certain. Therefore, only the direction of the minor axis is used to find the pole in a least squares solution, where n observations are used. We add these two intersecting great circle poles to Table 6.

Fig. 5 shows the great circles from the position of Ceres for each of the ten nights of AO observations in the direction of the average measured minor axes for the night, plotted on the celestial sphere (Fig. 5). In the first intersecting great circle method (a), the 45 intersections between each pair of great circles are converted to Cartesian coordinates and averaged to find a mean pole. Nine intersections more than 40° away from the average position are thrown out, and the remaining 36 intersections are then used to find a slightly different pole, but with half the uncertainty. The reason some intersections are so far away is that they are intersections from nearly parallel lines, from observations made close together in celestial or ecliptic coordinates. The standard deviations of the Cartesian coordinates of the 36 intersections are propagated to an uncertainty and shown as a circle around the final pole. The uncertainties of the coordinates from the least squares fit in the second method are converted to a radius and are also shown in Fig. 5.

In addition, the three poles from the recent work of Thomas et al. (2005), Drummond and Christou (2008), and Carry et al. (2008) also reported in Table 6 are indicated in Fig. 5. These authors derived the coordinates of Ceres' spin-axis using different techniques and data sets: Thomas et al. (2005) tracked the apparent motion of features across the disk of Ceres from HST images, Drummond and Christou (2008) used the intersection of great circles based on AO and HST images, and a stellar occultation, and Carry et al. (2008) also tracked features across the disk of Ceres on AO images acquired in 2002. The pole we derive here is 2° from Carry et al. (2008), and is 5° from the pole of Thomas et al. (2005).

5. Summary

The results reported here, including the possibility of a triaxial ellipsoid shape for Ceres, agree with the work of Carry et al. (2008), who used a subset of our AO data. The difference between our a and b dimensions are not significant because they are similar, to within their uncertainties, and both the triaxial ellipsoid and

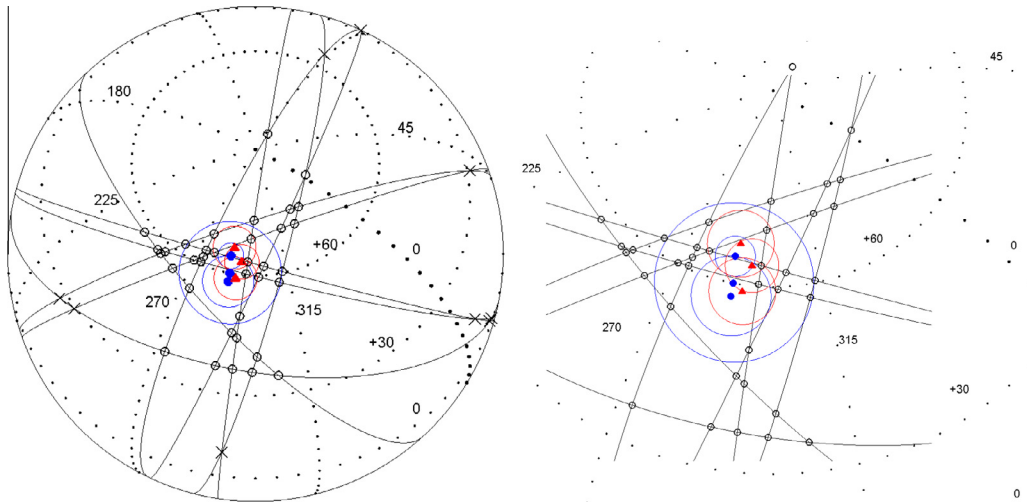


Fig. 5. Determination of Ceres' poles from the great circle methods (the right figure is a closeup of part of the left figure). Ten great circles, perpendicular to the average position angle of the long axis on each of ten nights of AO images, encircle the celestial sphere. Of the 45 intersections produced by the 10 circles, 36 are marked by a circle if they are used to form an average pole, or an X if not. The three poles we derive (Table 6) are marked with blue dots, and are encircled by their region of uncertainty. The three poles from the recent work of others (also in Table 6) are indicated by red triangles and their error radius of uncertainty. (For interpretation of the references to color in this figure legend, the reader is referred to the web version of this article.)

oblate spheroid fit the data with comparable residuals. This suggests that Ceres is indeed an oblate spheroid. We determine the coordinates of the spin vector to lie within 3° of $(287^\circ, +64^\circ)$ in an equatorial J2000 reference frame, for an obliquity of only 3° between it and Ceres' orbital pole. While still being within the error bars of recent determinations of the rotational pole by Carry et al. (2008) and Thomas et al. (2005), 2° and 5° away, respectively, we have improved the uncertainty from larger than 3° to now 3° . The orientation of the spin axis in space is therefore well-constrained, and will facilitate the early science planning of Dawn during its rendezvous with Ceres in 2015.

The introduction of a limb-darkening-like function, which we label a 'terminator fade', into our analysis significantly reduces the residuals of higher solar phase angle observations, especially for the equatorial diameter. We find that the dimensions for Ceres are 1–2% smaller than those from HST, while the oblateness is similar with both techniques.

Acknowledgments

This work was supported by research grants to our group (Merline PI) from the NASA Planetary Astronomy Program and

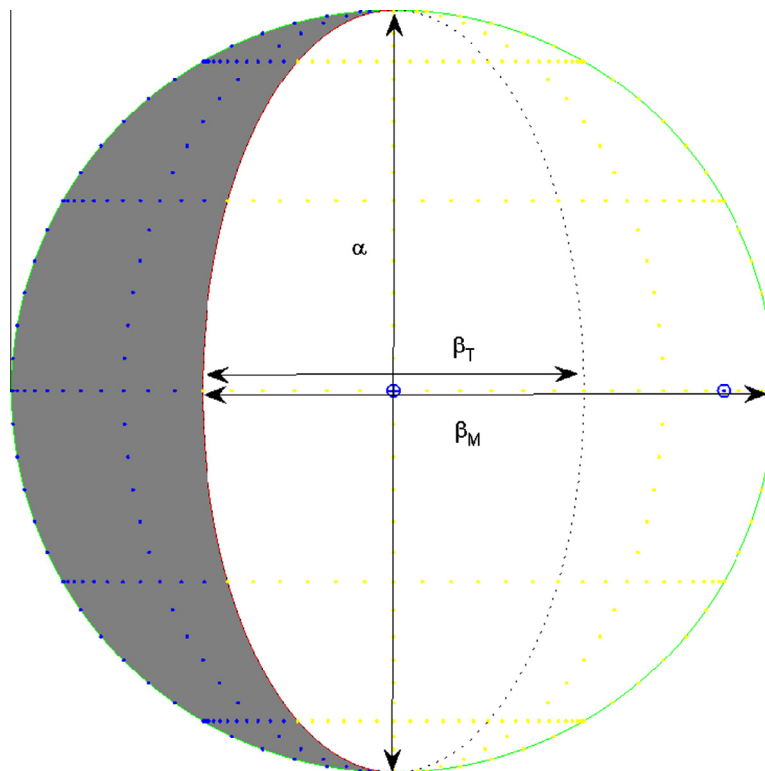


Fig. A.1. Spheroid case. For a spheroid, α is the major diameter, β is the minor diameter (which equals α in this example), β_T is the terminator ellipse diameter, and β_M is $(\beta + \beta_T)/2$. The sub-Earth point is denoted by \oplus and the sub-sun point is \odot . This terminator is for solar phase angle $\omega = 60^\circ$.

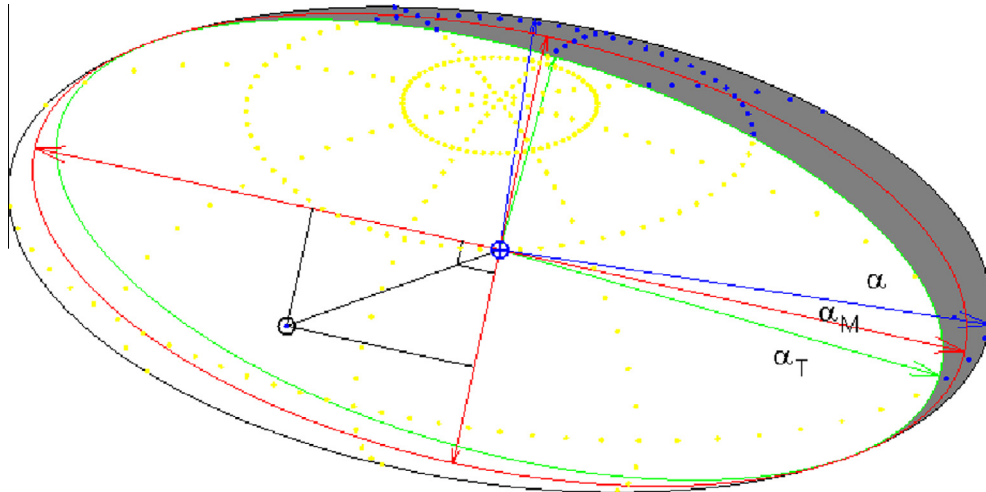


Fig. A.2. Illuminated and unilluminated portions of a $3 \times 2 \times 1$ triaxial ellipsoid. The major body dimension is α , α_t is the terminator ellipse dimension, and α_M is the mean ellipse dimension. The sub-Earth point is denoted by \oplus and the sub-sun point by \ominus , with a solar phase angle in this case of $\omega = 42^\circ$.

the NSF Planetary Astronomy Program. We also thank two referees for their careful readings and thoughtful suggestions which helped tighten up this paper. The authors wish to recognize and acknowledge the very significant cultural role and reverence that the summit of Mauna Kea has always had within the indigenous Hawaiian community. We are most fortunate to have the opportunity to conduct observations from this mountain. This research made use of NASA's Astrophysics Data System.

the details of the appearance of a triaxial ellipsoid under Sun–Earth geometry have previously been derived analytically, and include the terminator as a hard edge, here we derive an extra term for the softness of the terminator from geometrical considerations. This term seems to account for the departures of the size of Ceres under the standard assumptions.

Appendix A. Terminator fading

A.1. Introduction

Global fits of Ceres revealed the necessity to account for the undersized appearance of Ceres at solar phase angles $>10^\circ$. While

A.2. Spherical case

Assuming that an asteroid can be modeled as triaxial ellipse with diameters $a \geq b \geq c$ rotating about its c axis, it always presents an apparent ellipse with major and minor axes of $\alpha > \beta$. The terminator across the triaxial ellipsoid presents as half an ellipse with $\alpha_T > \beta_T$. Initially, for simplicity we will assume a spheroid (Fig. A.1) with diameters $a = b = c$. In Fig. A.1 the length

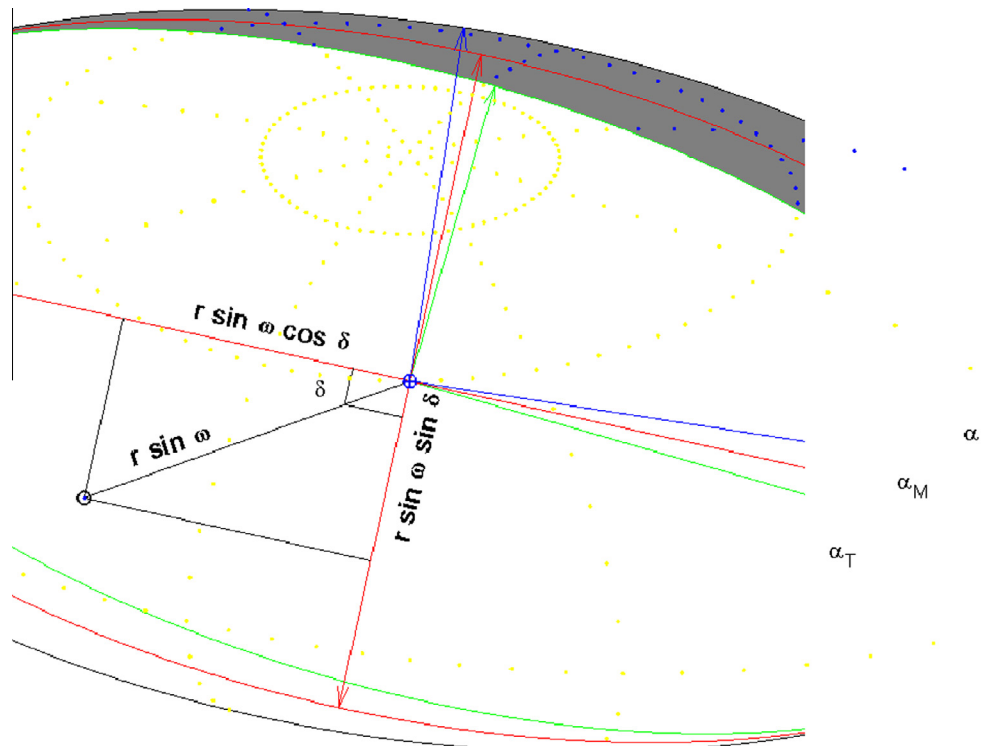


Fig. A.3. Closeup of Fig. A.2. The angle between the sun and the major illuminated axis is δ , and the smaller set of perpendiculars is from multiplying the larger set by $k = 0.2$.

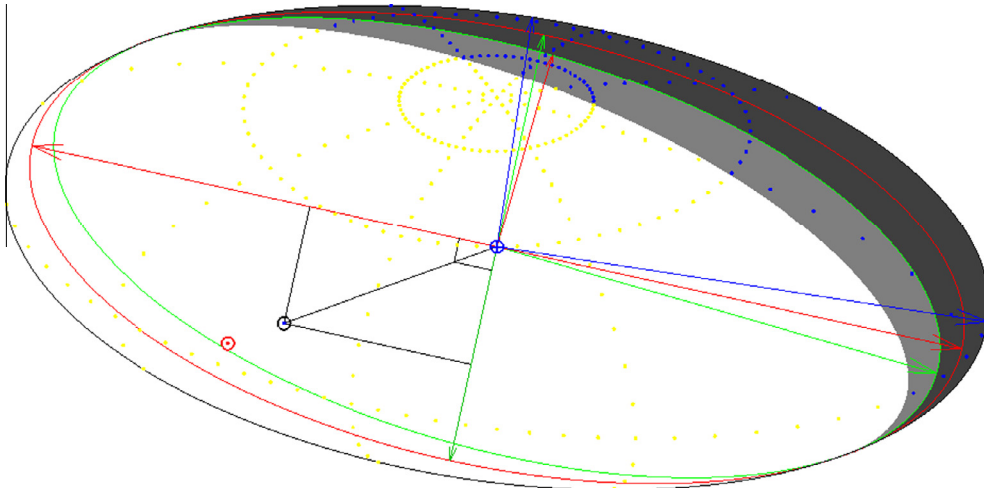


Fig. A.4. Same as Fig. A.2, but showing the effect of terminator fading. The lighter gray area represents the ‘soft’ region next to the true terminator, creating a new, pseudo-terminator. The red sun symbol shows the position of the Sun for the pseudo-terminator, and corresponds to an effective solar phase angle of $\omega_e = 52^\circ$ from Eq. (A.2). (For interpretation of the references to color in this figure legend, the reader is referred to the web version of this article.)

of the illuminated long axis α_M is simply $\alpha = \alpha_T$, while β_M , the illuminated mean minor diameter is

$$\beta_M = (\beta + \beta_T)/2 = (\beta + \beta \cos \omega)/2 = \beta(1 + \cos \omega)/2$$

where ω is the solar phase angle, and which shows that $\beta_T = \beta \cos \omega$. Thus, we want to compare our measured ellipse to the mean illuminated ellipse of

$$\alpha_M \times \beta_M = \alpha \times (\beta + \beta \cos \omega)/2.$$

A.3. Triaxial ellipsoid case

For the more general case of a triaxial ellipsoid, the body ellipse, $\alpha \times \beta$, and terminator ellipse, $\alpha_T \times \beta_T$, combine in a more complicated way to make a mean ellipse. Figs. A.2 and A.3 show an imaginary $3 \times 2 \times 1$ triaxial ellipsoid with a solar phase angle of 42° .

From Eq. (1), we have

$$\beta_O = \beta_M - kr \sin \omega \sin \delta. \quad (\text{A.1})$$

For small to moderate solar phase angles involved on a nearly spherical body, where the object’s diameter is $2r \simeq \alpha \simeq \beta$, its illuminated minor diameter would be $\beta_M = r + r \cos \omega$, and with Eq. (A.1), since $\delta = \pi/2$, $\beta_O = r + r \cos \omega - kr \sin \omega = r + r(\cos \omega - k \sin \omega)$. We can then define an effective solar phase angle as

$$\omega_e = \arccos(\cos \omega - k \sin \omega) \quad (\text{A.2})$$

to draw a pseudo-terminator in Fig. A.4 that demarcates a soft area between it and the true terminator. This pseudo-terminator defines one edge for our AO measurements.

References

- A’Hearn, M.F., Feldman, P.D., 1992. Water vaporization on Ceres. *Icarus* 98, 54–60.
- Carry, B., 2009. Asteroids physical properties from high angular-resolution imaging. Ph.D. thesis, Observatoire de Paris.
- Carry, B., 2012. Density of asteroids. *Planet. Space Sci.* 73, 98–118.
- Carry, B. et al., 2008. Near-infrared mapping and physical properties of the dwarf planet Ceres. *Astron. Astrophys.* 478 (4), 235–244.
- Carry, B. et al., 2010a. Physical properties of the ESA Rosetta target Asteroid (21) Lutetia. II. Shape and flyby geometry. *Astron. Astrophys.* 523, 19 pages. Article No: A94.
- Carry, B., Dumas, C., Kaasalainen, M., Berthier, J., Merline, W.J., Erard, S., Conrad, A., Drummond, J.D., Hestroffer, D., Fulchignoni, M., Fusco, T., 2010b. Physical properties of (2) Pallas. *Icarus* 205, 460–472.
- Carry, B. et al., 2012. Shape modeling technique KOALA validated by ESA Rosetta at (21) Lutetia. *Planet. Space Sci.* 66, 200–212.
- Castillo-Rogez, J.C., McCord, T.B., 2010. Ceres: Evolution and present state constrained by shape data. *Icarus* 205, 443–459.
- Chamberlain, M.A., Sykes, M.V., Esquerdo, G.A., 2007. Ceres lightcurve analysis period determination. *Icarus* 188 (2), 451–456.
- Chapman, C.R., McCord, T.B., Johnson, T.V., 1973. Asteroid spectral reflectivities. *Astron. J.* 78, 126–140.
- Conrad, A.R., Dumas, C., Merline, W.J., Drummond, J.D., Campbell, R.D., Goodrich, R.W., Le Mignant, D., Chaffee, F.H., Fusco, T., Kwok, S.H., Knight, R.I., 2007. Direct measurement of the size, shape, and pole of 511 Davida with Keck AO in a single night. *Icarus* 191 (2), 616–627.
- Drummond, J.D., 2000. Measuring Asteroids with Adaptive Optics. In: Ageorges, N., Dainty, C. (Eds.), *Laser Guide Star Adaptive Optics for Astronomy*, pp. 243–262.
- Drummond, J.D., Christou, J.C., 2008. Triaxial ellipsoid dimensions and rotational poles of seven asteroids from Lick Observatory adaptive optics images, and of Ceres. *Icarus* 197, 480–496.
- Drummond, J.D., Christou, J.C., Nelson, J., 2009a. Triaxial ellipsoid dimensions and poles of asteroids from AO observations at the Keck-II telescope. *Icarus* 202, 147–159.
- Drummond, J.D., Cocke, W.J., Hege, E.K., Strittmatter, P.A., Lambert, J.V., 1985. Speckle interferometry of asteroids. I. 433 Eros. *Icarus* 61, 132–151.
- Drummond, J.D., Conrad, A., Merline, W., Carry, B., 2009b. The Dimensions and Pole of Asteroid (21) Lutetia from Adaptive Optics Images. *AAS/Division for Planetary Sciences Meeting Abstracts* 41, # 59.07.
- Drummond, J.D. et al., 2010. Physical properties of the ESA Rosetta target Asteroid (21) Lutetia. I. The triaxial ellipsoid dimensions, rotational pole, and bulk density. *Astron. Astrophys.* 523, 8 pages. Article No: A93.
- Drummond, J.D., Fugate, R.Q., Christou, J.C., Hege, E.K., 1998. Full adaptive optics images of asteroids Ceres and Vesta; rotational poles and triaxial ellipsoid dimensions. *Icarus* 132, 80–99.
- Fanale, F.P., Salvail, J.R., 1989. The water regime of Asteroid (1) Ceres. *Icarus* 82, 97–110.
- Feierberg, M.A., Lebofsky, L.A., Larson, H.P., 1980. Spectroscopic evidence for aqueous alteration products on the surfaces of low-albedo asteroids. *Geochim. Cosmochim. Acta* 45, 971–981.
- Kaasalainen, M., et al., 2011. Shape reconstruction of irregular bodies with multiple complementary data sources. *EPSC-DPS Joint Meeting 2011* 416.
- Küppers, M. et al., 2014. Localized sources of water vapour on the dwarf planet (1) Ceres. *Nature* 505, 525–527.
- King, T.V., Clark, R.N., Calvin, W.M., Sherman, D.M., Brown, R.H., 1992. Evidence for ammonium-bearing minerals on Ceres. *Science* 255, 1551–1553.
- Kuchynka, P., Folkner, W.M., 2013. A new approach to determining asteroid masses from planetary range measurements. *Icarus* 222, 243–253.
- Lebofsky, L.A., 1978. Asteroid 1 Ceres – Evidence for water of hydration. *Mon. Not. R. Astron. Soc.* 182, 17–21.
- Lenzen R., 2003. NAOS-CONICA first on sky results in a variety of observing modes. *SPIE*, vol. 4841, pp. 944–952.
- Li, J.-Y., McFadden, L.A., Parker, J.W., Young, E.F., Stern, S.A., Thomas, P.C., Russell, C.T., Sykes, M.V., 2006. Photometric analysis of 1 Ceres and surface mapping from HST observations. *Icarus* 182, 143–160.
- Li, J.-Y., Thomas, P.C., Carcich, B., Mutchler, M.J., McFadden, L.A., Russell, C.T., Weinstein-Weiss, S.S., Rayman, M.D., Raymond, C.A., 2011. Improved measurement of Asteroid (4) Vesta’s rotational axis orientation. *Icarus* 211, 528–534.
- McCord, T.B., Sotin, C., 2005. Ceres: Evolution and current state. *J. Geophys. Res. (Planets)* 110, 5009–5023.
- Merline, W.J., Drummond, J.D., Carry, B., Conrad, A., Tamblyn, P.M., Dumas, C., Kaasalainen, M., Erikson, A., Mottola, S., Durech, J., Rousseau, G., Behrend, R.,

- Casalnuovo, Chinaglia, B., Christou, J.C., Chapman, C.R., Neyman, C., . The Resolved Asteroid Program – Size, shape, and pole of (52) Europa. *Icarus* 225, 794–805.
- Milliken, R.E., Rivkin, A.S., 2009. Brucite and carbonate assemblages from altered olivine-rich materials on Ceres. *Nat. Geosci.* 2, 258–261.
- Millis, R.L., Wasserman, L.H., Franz, O.G., Nye, R.A., Oliver, R.C., Kreidl, T.J., Jones, S.E., Hubbard, W.B., Lebofsky, L.A., Goff, R., Marcialis, R., Sykes, M.V., Frecker, J., Hunten, D., Zellner, B.H., Reitsema, H.J., Schneider, G.H., Dunham, E., Klavetter, J., Meech, K.J., Oswalt, T.D., Rafert, J., Strother, E.F., Smith, J.A., Povenmire, H.R., Jones, B., Kornbluh, D., Reed, L., Izor, K., A'Hearn, M.F., Schnurr, R.G., Osborn, W., Parker, D.C., Douglas, W.T., Beish, J.D., Klemola, A.R., Rios, M., Sanchez, A., Piironen, J., Mooney, M., Ireland, R.S., Leibow, D., 1987. The size, shape, density, and albedo of Ceres from its occultation of BD + 8°471. *Icarus* 72, 507–518.
- Parker, J.W. et al., 2002. Analysis of the first disk-resolved images of Ceres from ultraviolet observations with the Hubble Space Telescope. *Astron. J.* 123, 549–557.
- Rivkin, A.S. et al., 2011. The surface composition of Ceres. *Space Sci. Rev.* 163, 95–116.
- Rousselot, P. et al., 2011. A search for water vaporization on Ceres. *Astron. J.* 142, 6 pages. Article No: A125.
- Rousset et al., 2003. NAOS, the first AO system of the VLT: On-sky performance. *SPIE*, vol. 4839, pp. 140–149.
- Russell, C.T. et al., 2007. Dawn mission to Vesta and Ceres. *Earth Moon Planets* 101, 65–91.
- Russell, C.T. et al., 2012. Dawn at Vesta: Testing the protoplanetary paradigm. *Science* 336, 684–686.
- Thomas, P.C. et al., 2005. Differentiation of the asteroid Ceres as revealed by its shape. *Nature* 437, 224–226.
- van Dam, M.A., Le Mignant, D., Macintosh, B., 2004. Performance of the Keck Observatory adaptive-optics system. *Appl. Opt.* 43 (23), 5458–5467.
- Zolotov, M.Y., 2009. On the composition and differentiation of Ceres. *Icarus* 204, 183–193.